Int. J. Appl. Ceram. Technol., 7 [1] 30–40 (2010)
DOI:10.1111/j.1744-7402.2009.02413.x

International Journal of
Applied
Ceramic
TECHNOLOGY
Ceramic Product Development and Commercialization

Electrophoretic Codeposition of $La_{0.6}Sr_{0.4}Co_{0.8}Fe_{0.2}O_{3-\delta}$ and Carbon Nanotubes for Developing Composite Cathodes for Intermediate Temperature Solid Oxide Fuel Cells

Maria J. Santillán

Comisión Nacional de Energía Atómica, CONICET, Centro Atómico Bariloche and Instituto Balseiro, 8400 S. C. de Bariloche, Argentina

Alberto Caneiro

Comisión Nacional de Energía Atómica, CONICET, Centro Atómico Bariloche and Instituto Balseiro, 8400 S. C. de Bariloche, Argentina

Francisco C. Lovey

Comisión Nacional de Energía Atómica, CONICET, Centro Atómico Bariloche and Instituto Balseiro, 8400 S. C. de Bariloche, Argentina

Nancy Quaranta

CIC Researcher, FR San Nicolás, Universidad Tecnológica Nacional, 2900 San Nicolás, Argentina

Aldo R. Boccaccini*

Department of Materials, Imperial College London, Prince Consort Road, London SW7 2BP, United Kingdom

*a.boccaccini@imperial.ac.uk

Carbon nanotubes (CNTs)/$La_{0.6}Sr_{0.4}Co_{0.8}Fe_{0.2}O_{3-\delta}$ (LSCF) composite films have been fabricated by electrophoretic codeposition on $Ce_{0.9}Gd_{0.1}O_{1.95}$ (CGO) substrates. CNTs are used as a sacrificial phase to produce ordered porous LSCF cathodes for intermediate temperature solid oxide fuel cells. The synthesis of LSCF powder by a modified sol–gel route is presented. The possible mechanism of formation of CNT/LSCF composite nanoparticles in suspension is discussed. Moreover the optimal suspension composition and the conditions for achieving successful electrophoretic deposition (EPD) of CNTs/LSCF composite nanoparticles were evaluated. Experimental results showed that the CNTs were homogeneously distributed and mixed with LSCF nanoparticles forming a mesh-like structure, which resulted in a highly porous LSCF film when the CNTs were burned out during heat treatment in air at 800°C for 2 h. Scanning electron microscopy (SEM), transmission electron microscopy (TEM), and X-ray diffraction (XRD) techniques were employed to characterize the microstructure of the precursors and of the composite films.

Introduction

Solid oxide fuel cells (SOFCs) are recognized as a leading and promising technology to offer clean and efficient power sources with reduced emission of pollutants.[1] The employment of new electrolyte materials such as $Ce_{0.9}Gd_{0.1}O_{1.95}$ (CGO) enables the reduction of the SOFC operating temperature below 700°C, which gives rise to so-called intermediate temperature-SOFC (IT-SOFC).[2,3]

The perovskite $La_{0.6}Sr_{0.4}Co_{0.8}Fe_{0.2}O_{3-\delta}$ (LSCF) is one of the most promising cathode materials for IT-SOFC, with excellent mixed ionic–electronic conductivity, high electrocatalytic activity and exhibiting low chemical reactivity and thermal expansion coefficient (TEC) similar to the CGO electrolyte.[4,5] Many efforts over the last years have been devoted to improve the electrochemical performance of IT-SOFC cathodes. The cathode performance is highly influenced by the material route preparation and the control of the cathode microstructure. In this context, it is a common procedure to control the microstructure of the cathode in order to enhance the reaction zone for the electrochemical reduction of molecular oxygen. The presence of small grains and a porous microstructure extend the electrode reaction beyond the triple phase boundary with the consequent reduction of the polarization resistance.[6] For this purpose, nanostructured materials and composite cathodes have been developed.[7–10]

Carbon nanotubes (CNTs) have attracted much attention since the first systematic investigation by Iijima[11] due to their excellent mechanical and electrical properties as well as remarkable chemical stability, according to their graphitic structure.[12] CNTs could also be used as sacrificial templates for the fabrication of porous ceramic materials with controlled nanoporosity.

In this investigation, we suggest that the combination of CNTs and LSCF nanoparticles could be an attractive approach to improve the electrochemical performance of SOFC cathodes due to the increment of the cathode's porosity when CNTs are used as sacrificial phase to create pores.

Electrophoretic deposition (EPD) has become a prominent alternative processing technique with great potential for the production of SOFCs components[13] in comparison with other methods such as laser ablation deposition,[7] pulsed laser deposition,[14] molecular beam epitaxy,[15] dip coating,[16] and spray coating.[17]

EPD is a two-step colloidal process that occurs under the effect of externally applied electric field on particles in a liquid suspension. Firstly, when the electric field is applied to charged particles, these migrate toward the working electrode of opposite charge. In the second step the charged particles coagulate on the surface of the working electrode, obtaining as a result a solid deposited film.[18] EPD is a versatile material processing method involving low cost and simple apparatus, which allows high microstructural control of coatings on substrates with complex shapes, manipulating experimental variables such as the applied voltage and deposition time.[13,18,19]

There has been previous interesting research considering the use of EPD in the SOFC field. For example, the preparation of dense layers of LSCF on a porous tubular alumina substrate using EPD was achieved by Negishi *et al.*[20] Moreover, Zhitomirsky and Petric[21] reported the EPD of perovskites and CGO on Ni–YSZ substrates and Ni foils. Further work on EPD for SOFC development has been presented at the previous EPD international conference.[22]

EPD has been also applied successfully to manipulate and deposit CNTs in ordered structures.[23,24] Moreover, the combination of CNTs and ceramic

nanoparticles (e.g. TiO_2, SiO_2) by EPD has been also demonstrated.[25,26] Recently, composites of CNTs and Fe_2O_3 nanocrystals have been developed by EPD for future applications in luminescent, magnetic, and energy-storage devices.[27] Our previous investigation[28] has shown that EPD is also an attractive technique for obtaining LSCF cathodes directly deposited on non-conducting CGO electrolyte substrates.

In the present work, we have investigated the electrophoretic codeposition (co-EPD) of LSCF nanoparticles and CNTs (CNTs/LSCF) for fabrication of composite cathodes on CGO electrolyte. The CNTs should act as sacrificial template (pore-forming elements) leading to tailored porous LSCF cathodes upon heat-treatment when CNTs are burnt out.

Experimental Procedures

Starting Materials

The LSCF powders were prepared by a sol–gel route as explained below (section Preparation of LSCF Powders). Acetylacetone (AcAc) (Merck, Whitehouse Station, NJ) was used as the solvent and iodine 99.999% (Merck) was used as a charge promoter, following our previous investigation.[28] Commercial multiwalled CNTs (Alfa Aesar, Ward Hill, MA; Karlsruhe, Germany) of $\sim$200 μm length and an external average diameter of 15 nm were used in this investigation.

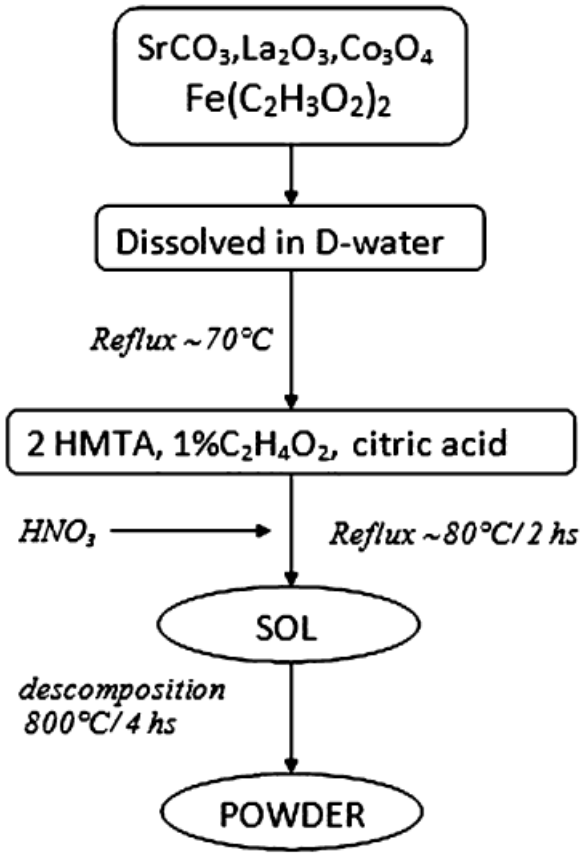

Fig. 1. Flow chart for the preparation of $La_{0.6}Sr_{0.4}Co_{0.8}Fe_{0.2}O_{3-\delta}$ powders.

Preparation of LSCF Powders

The LSCF powders were prepared by a modified sol–gel route[29] using $SrCO_3$, La_2O_3, Co_3O_4, and Fe acetate [$(C_2H_8)_3Fe_2$] as starting materials. The experimental procedure is schematically shown in Fig. 1. Briefly, appropriate quantities of reagents were dissolved in distilled water. All the solutions were homogenized at 70°C. After that, 2% of hexamethylenetetramine (HMTA), 1% of ethylene glycol ($C_2H_6O_2$) and citric acid were added to promote the polyesterification and polycondensation reactions. HMTA controls the particle size during the gelation process and also prevents the aggregation of particles during the thermolysis of dry gel due to its sterostructure. Citric acid acted as chelating agents to Fe^{3+} source in a ratio <3[30] in order to obtain homogeneous polymeric sols. The volume of the solution was adjusted to 200 mL by addition of nitric acid. The system was maintained in reflux for 2 h. A dark red resin was obtained upon drying at 100°C. Powders were finally synthesized by the sol calcination at 450°C in air followed by heat treatment at 800°C in air for a period of 4 h. The presence of single-phase materials was confirmed by powder X-ray diffraction (XRD) analysis.

Preparation of LSCF–CNTs Suspension and Electrodes for EPD

The preparation of the suspensions for EPD consisted of a two-step procedure. Firstly, 0.5 g of CNTs were oxidized using a HNO_3 and H_2SO_4 mixture (ratio 3:1) in reflux at 130°C for 30 min. To give them a negative surface charge due to dissociation of COOH groups presents on it, as it is well known from the literature.[23,26,31] After that, CNTs were washed several times in distilled water up to pH $\sim$7. Then, the suspension was centrifuged at

2000 rpm for 15 min to remove any agglomerates which would affect the microstructure of the films.

In order to obtain stable suspensions for the homogeneous electrophoretic codeposition of CNTs/LSCF on the CGO pellets, several experiments were carried out using suspensions with different relative proportions of CNTs and LSCF nanoparticles (1:40, 1:15, 1:10, 1:5, and 1:1). These suspensions were prepared by adding oxidized CNTs to suspensions of dispersed LSCF nanoparticles and iodine in AcAc. The concentration of LSCF in the base suspension was always 0.1wt%. These suspensions were ultrasonically mixed for 3 h before the EPD process.

Dense pellets of the $Ce_{0.9}Gd_{0.1}O_{1.95}$ (CGO) electrolyte were used as deposition substrate. These were obtained by uniaxial pressing CGO powder (Praxair Surface Technologies, Indianapolis, IN). Green pellets of 13 mm in diameter and 1.1 mm thickness were sintered at 1360°C for 6 h in air. The final diameter of the CGO pellets used as electrode was ~12.5 mm. Before EPD the surface of the substrate was polished using diamond paste and covered with a thin film of silver by sputtering.

The EPD process was carried out using constant voltage in the range 5–30 V. The deposition time was varied from 1 to 6 min. To achieve a simultaneous deposition in both faces of the CGO substrate, the EPD cell included the CGO pellet used as cathode centered between two parallel planar stainless-steel counter-electrodes (anode) with 5 cm^2 of working area separated a distance of 1 cm.

After the EPD process, the samples were carefully removed from the EPD cell. They were horizontally dried in a desiccator at room temperature for 48 h. Then, the samples were heat-treated at 450°C in Ar with a flow rate of 20 mL/min for 1 h, and sintered at 800°C in air for 2 h, in order to promote the adhesion of the LSCF coating to the CGO substrate.

Characterization Techniques

The microstructure of the synthesized LSCF powders and coatings was observed by scanning electron microscopy, using a SEM Philips 515 equipped with EDX analysis (EDAX Genesis 2000 spectrometer, Philips, Eindhoven, The Netherlands).

XRD analysis was used for phase identification of the LSCF powders. The patterns were collected in the $20 \leq 2\theta \leq 70^\circ$ range with scan steps of 0.02° using a Phillips PW 1700 diffractometer equipped with a graphite monochromator and Cu$K\alpha$ radiation. Transmission electron microscopy (TEM) (Philips CM200 UT operated at 200 kV) was used for morphological characterization of the CNTs.

Results and Discussion

Starting Materials

The synthesized LSCF powders were analyzed by XRD to check phase purity and constitution; it was determined that XRD peaks of these powders completely matched the LSCF phase (space group: *R-3c*)[32] peaks, and no other crystalline phases were detected, as shown in Fig. 2. The inset in Fig. 2 shows one distinctive peak corresponding to the LSCF phase ($2\theta \sim 33^\circ$). The crystallite size estimated was $D \sim 22$ nm by using the Scherer equation; $D = K\lambda/(B\cos\theta)$ where $K = 0.9$ and B is the peak width, obtained using a Lorenzian peaks fitting routine. This result was analogous to the one obtained applying the Rietveld method using an isotropic size model. A SEM image of the LSCF particles is shown in Fig. 3. The powder appears to be highly agglomerated possibly due to the effects of surface tension and van-der-Waals interactions during milling and drying.

In Fig. 4a and b, TEM micrographs of the as-received multiwalled CNTs at different magnifications are shown, which reveal CNT diameters of ~15 nm and lengths of several microns. Fig. 4c) shows the HRTEM migrograph of a CNT. The number of the walls counted from the two sides of the tubes was not identical. Moreover, it is observed that the wall

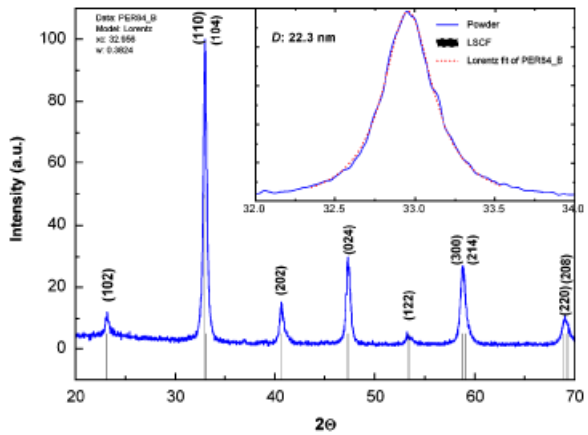

Fig. 2. X-ray diffraction (XRD) patterns of sol–gel derived $La_{0.6}Sr_{0.4}Co_{0.8}Fe_{0.2}O_{3-\delta}$ (LSCF) powder obtained after decomposition and calcination at 800°C (4 h) of the gel.

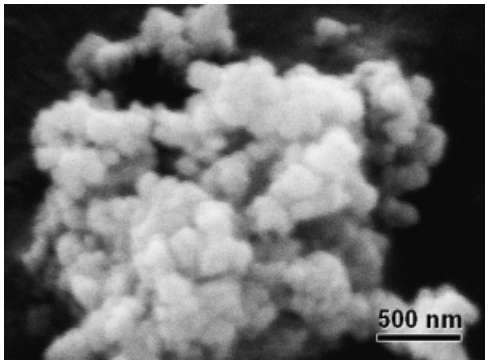

Fig. 3. Scanning electron microscopic (SEM) micrograph of $La_{0.6}Sr_{0.4}Co_{0.8}Fe_{0.2}O_{3-\delta}$ powder calcined at 800°C for 4 h.

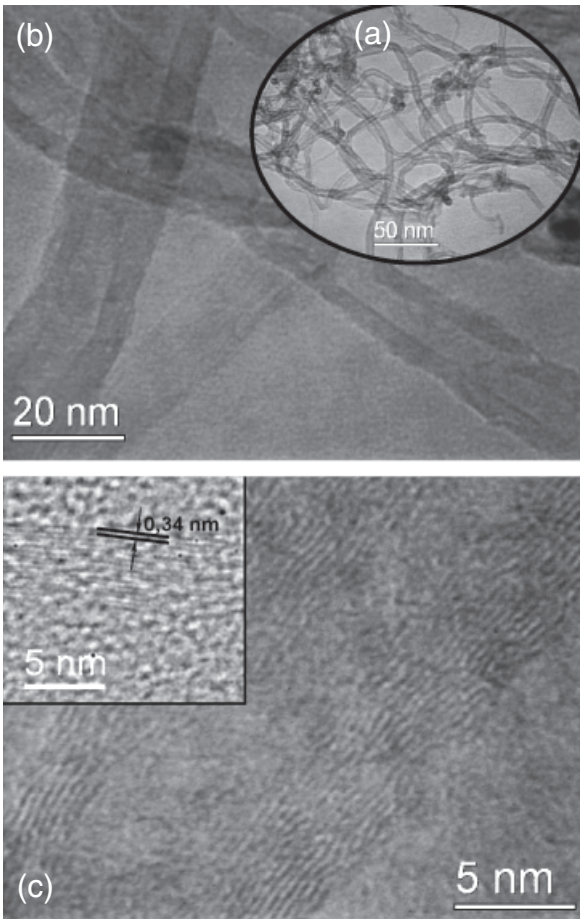

Fig. 4. (a–b) Transmission electron microscopy (TEM) micrograph of the as-received entangled multiwalled carbon nanotubes (CNTs). (c) HR-TEM micrograph of CNTs showing walls structure and details of the walls (shown in the inset).

thickness generally varied along the CNT length. The left inset in Fig. 4c) is an enlarged image of the tube wall. Fourier transform indicated that the distance between the graphene sheets is about 3.4 Å a value which corresponds well with reported values for this nanostructure.[33]

Fabrication of CNTs/LSCF Composite by Electrophoretic Codeposition

In the fabrication of a homogeneous coating by EPD a critical step is the preparation of a stable suspension with two or more different components aiming at achieving a homogeneous distribution of the particles during the coagulation of the species on the substrate, preventing preferential coagulation of one kind of particles. Therefore, it is essential in the present case which involves two very different species such as CNT and LSCF particles to consider the size of LSCF particles in relation of the CNTs size and the effect of the additives and solvent.

Numerous types of solvents have been used to prepare CNTs suspensions for EPD, including distilled water,[34] mixtures of acetone and ethanol,[24] and isopropyl alcohol,[35] among others, as reviewed elsewhere.[23]

In nonaqueous dispersions, the ionization of surface groups and adsorption of ionic surfactants are possible mechanisms for dispersion stability, for example, exploiting electrostatic and esteric stabilization, respectively.[18] In the present work, AcAc was used as suspension medium for EPD. Our recently published investigation has determined the EPD parameters for a stable and well-dispersed suspension of LSCF powders in AcAc.[28] Other investigations have shown that iodine-dissolved AcAc is an effective agent of charge transference for EPD process.[36–39] Similar effects have been reported for solvents as acetone, ethanol, and other alcohols.[40]

A hypothesis for explaining the process of codeposition of CNTs/LSCF from the iodine containing AcAc suspensions developed in this study is presented next. CNTs previously treated with concentrated and hot HNO_3 and H_2SO_4 acids will exhibit a negative surface charge originated in the dissociation of COOH groups on their surface.[23,31,41] The acidic groups stabilize electrostatically the CNTs in polar solvents.[41] These functional groups will be useful for future chemical reaction with charged nanoparticles. On the other hand, when iodine is added in AcAc, iodine dissolved in this solvent has a low resistance and the LSCF nanoparticles become positively charged due to the absorption of H^+ on their

surface.[28] The H^+ are generated by the reaction between AcAc and iodine according to the reaction:[38,39]

$$CH_3CH_2COCH_2COCH_2CH_3 + 2I_2 \leftrightarrow ICH_2CH_2COCH_2COCH_2CH_2I + 2I^- + 2H^+ \quad (1)$$

Consequently, on addition of preoxided CNTs into the LCSF suspension, positively charged LSCF nanoparticles are attracted to the negatively charged CNTs. This mechanism should lead to the formation of individual CNTs/LSCF composite entities, which can migrate towards the cathode (negative electrode) under an external applied voltage, as they retain on overall positive charge. The self-assembly of particles of different charge in suspension for EPD has been proposed in the past, for example, for silica and alumina particles to form mullite[42] and in ZrO_2/MgO systems.[43]

The effect of the I_2 concentration on the production of protons and their adsorption on the CNTs/LSCF composite was investigated. According to Eq. (1), the amount of free H^+ increases with the raise of the I_2 concentration, resulting in a reduction of the pH value of the suspension, as shown in Fig. 5 for the CNTs/LSCF-suspension system. As a result, the mobility of free H^+ is far higher than that of the charged CNTs/LSCF composite entities. Consequently, an excess amount of I_2 will enhance proton migration and thus decrease the amount of CNTs/LSCF deposited. Therefore, by trial and error we have chosen a suspension with an I_2 concentration of 2.45 wt‰ with respect to the LSCF concentration and with pH ≈ 4.8, which gives the best deposition rate (2.43 mg/cm^2) applying 25 V for 4 min. These deposition conditions will be further discussed below. Under this condition, the amount of free protons should be negligible and CNTs/LSCF composite particles are the most important charge carriers in the suspension.

A similar explanation has been given for the electrophoretic codeposition of other systems combining CNTs and ceramic particles, such as TiO_2, SiO_2, and hydroxyapatite[25,26] when charged nanoparticles are attached to CNTs. A scheme of the electrophoretic codeposition process is shown in Fig. 6 where composite CNTs/LSCF nanoparticles, in this case positively charged, move towards the cathode when the external electric field is applied.

For the optimization of EPD parameters the experiments were conducted at different constant voltages for diverse time periods. Figure 7 shows the time-dependent variation of deposited weight at different applied voltages. After a trial-and-error approach, the optimal EPD parameters were found to be 25 V applied during 4 min. During the EPD process, the current decreased from 180 to 90 μA/cm^2 and then it remained constant. The electric field has a strong influence on deposition rate and on the microstructural homogeneity of the

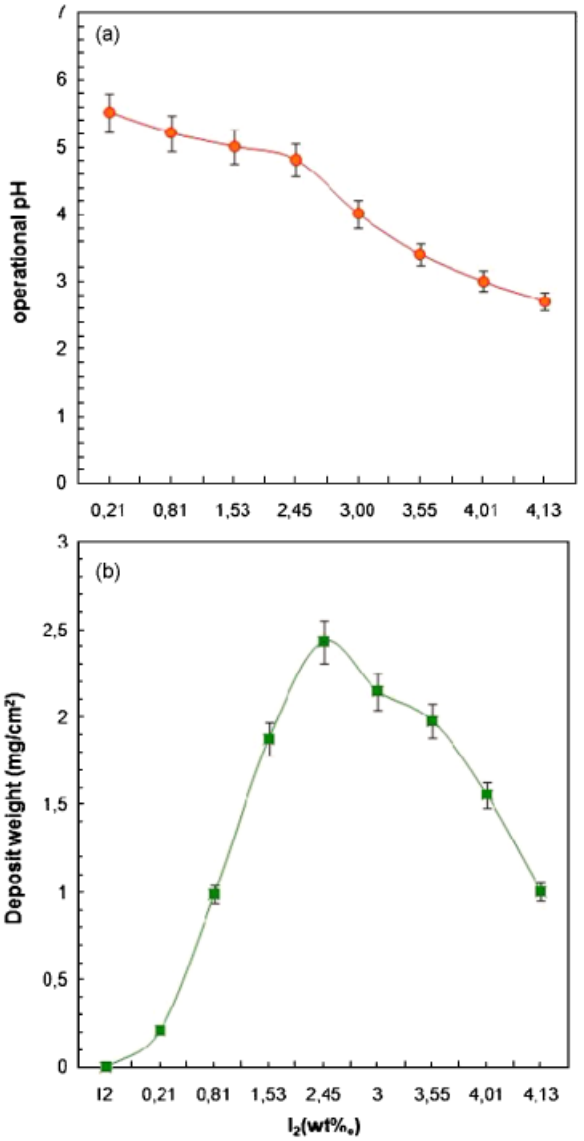

Fig. 5. The effect of I_2 concentration [referred to the concentration of $La_{0.6}Sr_{0.4}Co_{0.8}Fe_{0.2}O_{3-\delta}$ (LSCF powder)] in the Acetylacetone (AcAc) suspension on (a) operational pH and (b) deposited weight of carbon nanotubes (CNTs)/LSCF (1:10 ratio) at 25 V for 4 min.

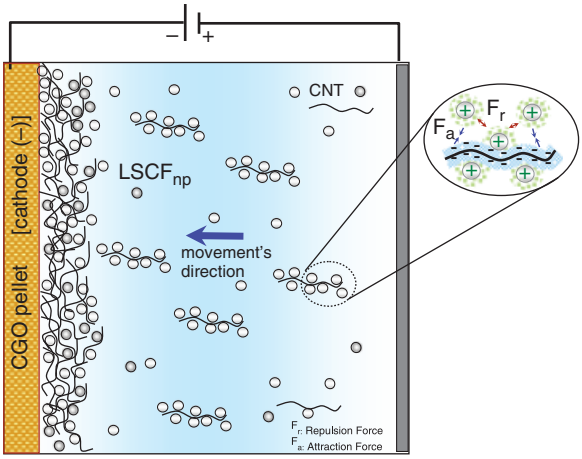

Fig. 6. Schematic diagram describing the electrophoretic co-deposition process of carbon nanotube (CNTs)/ $La_{0.6}Sr_{0.4}Co_{0.8}Fe_{0.2}O_{3-\delta}$ (LSCF) composite coating on CGO electrolyte.

films. When films were grown applying voltages <20 V, the deposits obtained were nonuniform exhibiting low density and the presence of some agglomerates, as seen in Fig. 8. This result is probably due to a lower electrophoretic mobility of the CNTs/LSCF composite particles and the consequently nonuniform coagulation on the substrate.

In general, it is expected that the applied voltage will have a significant influence on the final microstructure of the deposit, considering that the mobility of the

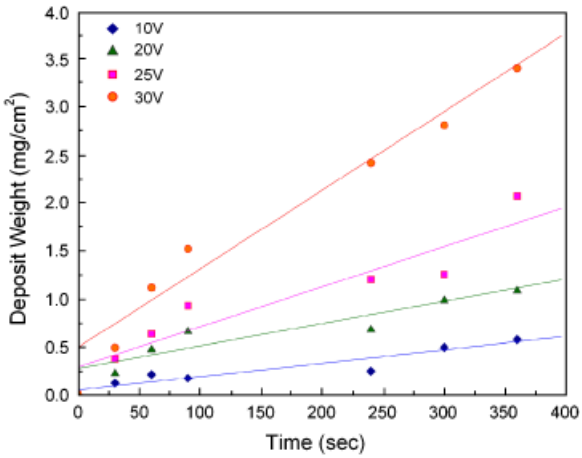

Fig. 7. Plots of the deposit weight versus time for different applied voltages using AcAc suspension with carbon nanotubes (CNTs)/ $La_{0.6}Sr_{0.4}Co_{0.8}Fe_{0.2}O_{3-\delta}$ (LSCF) (1:10 ratio).

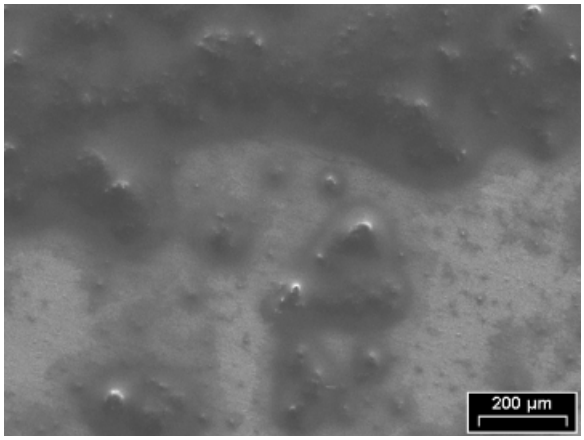

Fig. 8. Scanning electron microscopy (SEM) micrograph showing the top surface of a carbon nanotube (CNTs)/$La_{0.6}Sr_{0.4}Co_{0.8}Fe_{0.2}O_{3-\delta}$ (LSCF) composite coating obtained by electrophoretic deposition (EPD) at 15 V during 4 min. The formation of agglomerates can be identified due to nonuniform deposition at this relatively low voltage.

particles during EPD is related to the particle velocity per unit field and that the particle velocity can be expressed in terms of the charge of the particles and the applied electric field, as given by the Debye–Hückel equation:[44]

$$v = \mu E = \frac{2 \in \zeta}{3\eta} \quad (2)$$

where μ is the electrophoretic mobility, E is the applied electric field, η the viscosity of the suspension, $\in$ the dielectric permittivity of the medium and ζ is the zeta-potential.

For applied voltages higher than 25 V, the film microstructure was nonuniform, probably due to the presence of high concentration of H^+ ions in suspension that have high electrophoretic mobility, therefore competing with the CNTs/LSCF composite particles as charge carriers as mentioned above. This behavior is frequently discussed in the EPD literature[19,45,46] and it could explain our experimental results. Figure 9 illustrates the effect of LSCF particle concentration on the deposition rate for different voltages and for a deposition time of 4 min. The I_2 concentration was 2.45 wt‰ with respect to the LSCF concentration. As shown, with increasing concentration of LSCF nanoparticles, the deposition rate decreases for a given applied voltage, as it is usually expected. During the increase of LSCF particle concentration, the electrophoretic mobility of the CNTs/LSCF composite entities in suspension decreases because the H^+ concentration

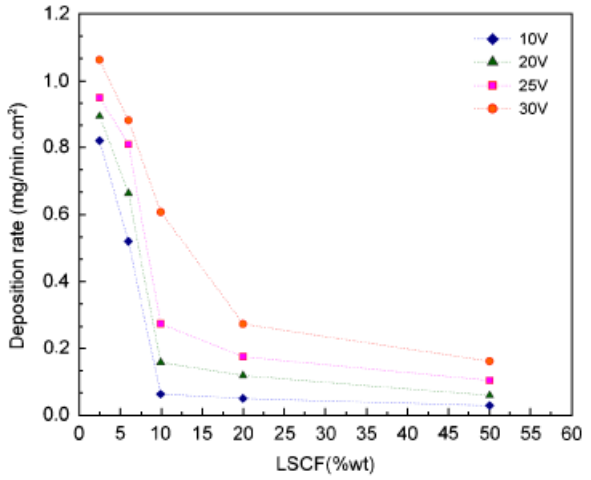

Fig. 9. Effects of $La_{0.6}Sr_{0.4}Co_{0.8}Fe_{0.2}O_{3-\delta}$ (LSCF) concentration on deposition rate for different applied voltages and deposition time of 4 min. (The I_2 concentration was 2.45 wt‰ with respect to the LSCF concentration).

produced by the reaction indicated in Eq. (1) remains constant, indicating that the charge available to be adsorbed on the CNTs/LSCF composite nanoparticles decreases, due to the presence of "free" LSCF particles. This reduced driving force for the electrophoretic phenomenon of CNTs/LSCF entities would lower the deposition rate. Alternatively, one can also consider that the effect of a lower concentration of LSCF particles in suspension is to increase the H^+ concentration available per CNTs/LSCF composite entity, improving thus their deposition rate.

After deposition, the samples were carefully removed from the EPD suspension for preventing the shedding of the coating on the substrate. This step was found to be critical for maintaining the integrity of the deposit over the whole substrate. When colloidal methods (i.e., EPD) are used to fabricate ceramic films, cracks can form as the film is dried due to the drying solvent inducing capillary stresses in the film. Because of constraints imposed by the substrate, these stresses, which would normally be alleviated by green body shrinkage can be sufficient to generate microcracks, for example, when the drying stresses exceed the cohesive force of the green ceramic film, the film fractures (cracks).

The quality of the produced CNTs/LSCF composite coatings was studied by visual inspection and SEM observations for films produced from suspensions with different concentrations of CNTs/LSCF particles. Visual observation of the films surface revealed that the superficial morphology of the coatings changes strongly with the concentration of CNTs/LSCF composite particles in suspension. The best quality films were obtained from suspensions of CNTs and LSCF nanoparticles containing a 1:10 weight ratio (CNT:LSCF nanoparticles) as mentioned before. These films exhibited a homogenous distribution of CNTs and LSCF nanoparticles before the heat-treated process at 450°C, which enabled to maintain the CNTs structure, as shown in Fig. 10. The CNTs were seen to remain predominantly parallel to the CGO substrate with an arbitrary in-plane orientation producing a porous mesh type structure. This effect is convenient for films to be employed as IT-SOFC cathodes because of the

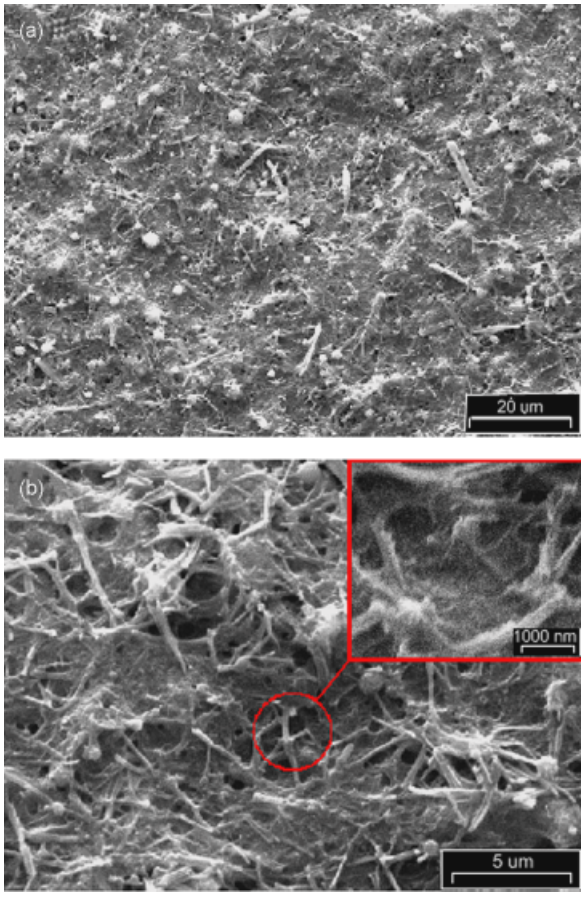

Fig. 10. Scanning electron microscopy (SEM) micrographs at different magnifications of top view of carbon nanotubes (CNTs)/ $La_{0.6}Sr_{0.4}Co_{0.8}Fe_{0.2}O_{3-\delta}$ (LSCF) composite coating obtained by electrophoretic deposition (EPD) at 25 V for 4 min and presintered (450°C, 1 h).

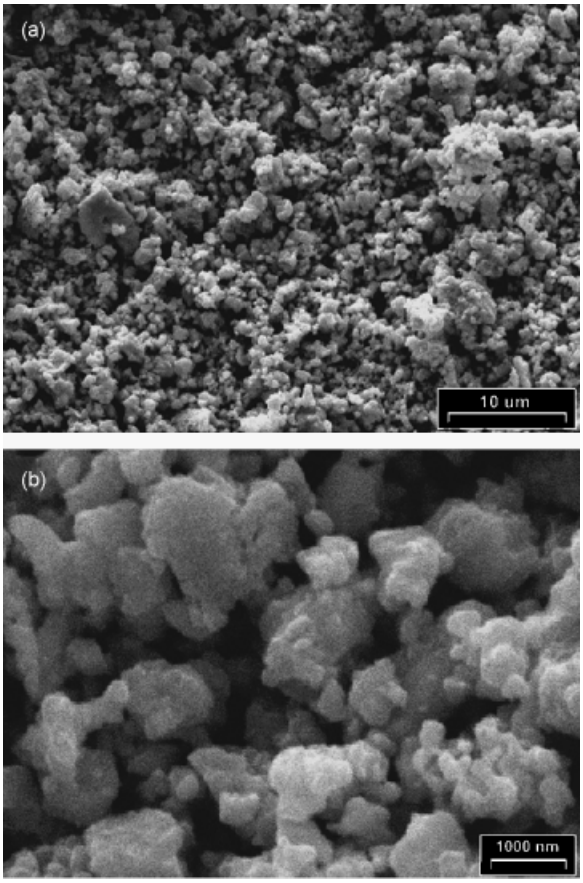

Fig. 11. Scanning electron microscopy (SEM) micrographs at low and high magnification of top view of carbon nanotubes (CNTs)/ $La_{0.6}Sr_{0.4}Co_{0.8}Fe_{0.2}O_{3-\delta}$ (LSCF) composite coating obtained by electrophoretic deposition (EPD) at 25 V for 4 min after heat-treatment at 800°C during 1 h in air.

possibility of developing large porosity (on burning out the CNTs) which would lead to a lower polarization resistance of the film. After sintering at 800°C for 1 h CNTs were no longer visible because they were burned out at high temperatures, giving a microstructure with high porosity, as shown in Fig. 11. As expected, it was observed that the porosity of cathodes made from CNTs/LSCF suspensions was much higher than that of cathodes obtained from suspensions of only LSCF (Fig. 12), as can be assessed qualitatively comparing the SEM micrographs in Figs 11 and 12. The XRD pattern of LSCF/CGO/LSCF symmetric cells is shown in Fig. 13. Only reflections corresponding to LSCF and CGO phases (space group: *Fm3m*) are present, suggesting that there was no chemical reaction between the LSCF film and the CGO substrate. It can be seen that some peaks of LSCF phase and CGO phase are overlapped. This resulting microstructure surely could influence the cathodic performance, which is limited by its microstructure and porosity,[47,48] which in turn depend on the preparation route of the nanoparticle LSCF powder and the EPD conditions. The oxygen reduction reaction mechanisms of the cathodes developed here will be reported in following papers.

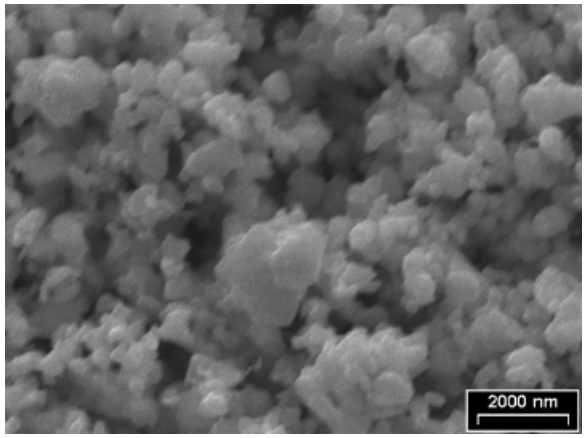

Fig. 12. Scanning electron microscopy (SEM) micrograph of a cathode obtained by electrophoretic deposition (EPD) using $La_{0.6}Sr_{0.4}Co_{0.8}Fe_{0.2}O_{3-\delta}$ (LSCF) powder only.

For 1:1 and 1:5 weight ratios of CNTs to LSCF nanoparticles in suspension, the films show evidence of poor deposition and lack of adherence to the CGO

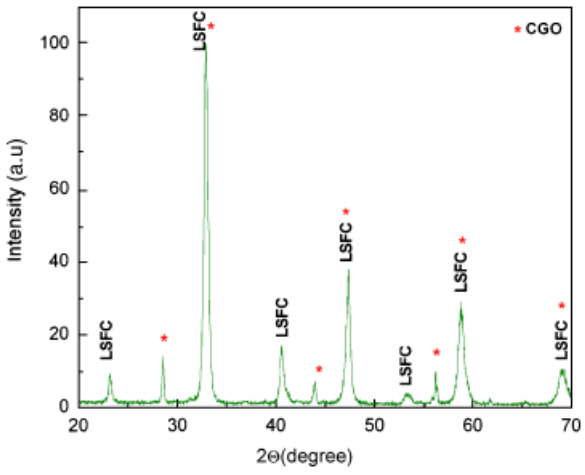

Fig. 13. X-ray diffraction (XRD) pattern of symmetric cell [$La_{0.6}Sr_{0.4}Co_{0.8}Fe_{0.2}O_{3-\delta}$ (LSCF)/CGO/LSCF] fabricated by electrophoretic deposition (EPD) of carbon nanotubes (CNTs)/ LSCF composite particles, sintered at 800°C for 1 h in air.

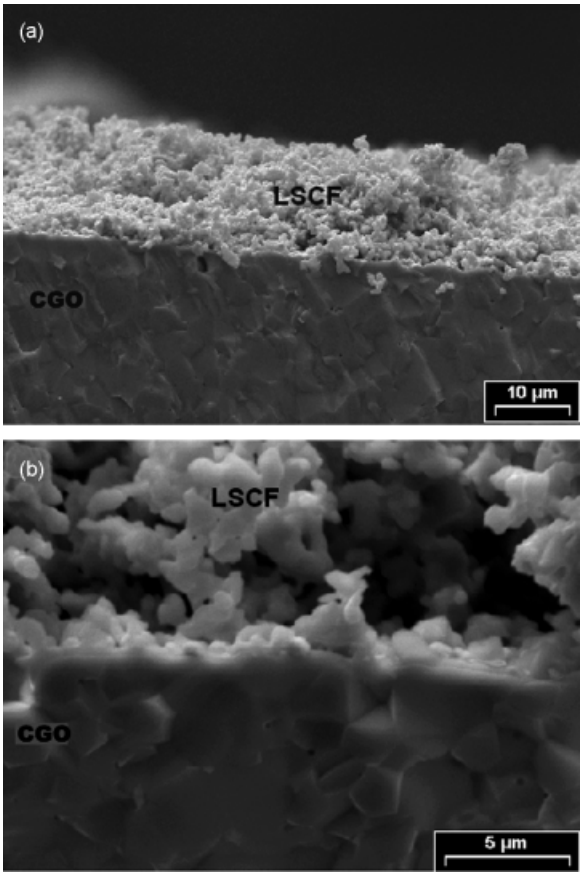

Fig. 14. Cross section of $La_{0.6}Sr_{0.4}Co_{0.8}Fe_{0.2}O_{3-\delta}$ (LSCF) films on CGO substrates obtained by electrophoretic deposition (EPD) of carbon nanotubes (CNTs)/LSCF composites, after heat-treatment at 800°C for 1 h.

substrate. On the other hand, CNTs/LSCF suspensions in ratios of 1:15 and 1:40 achieved films with high agglomeration level of LSCF nanoparticles, while the CNTs were well attached on the substrate surface. As mentioned above, the best microstructure quality of films was obtained from the suspension with CNTs/LSCF ratio 1:10 when a constant voltage of 25 V was applied during 4 min.

The thickness of the deposits was varied between 0 and 20 µm by variation of the deposition time and applied voltage in the working range indicated above. In cross-section SEM micrographs the obtained highly porous coating with uniform thickness (~20 µm) can be observed in Fig. 14a and very good bonding to the substrate can be inferred from the micrograph. The high magnification micrograph of the cross-section (Fig. 14b) clearly shows the porous nature of the coating.

Conclusions

EPD was applied for the first time to fabricate CNTs/LSCF composite films on dense nonconducting CGO substrates to be used as starting materials for cathodes in IT-SOFC. The composition of the diphasic starting suspensions (CNTs/LSCF) in AcAc with addition of iodine was investigated for cathodic EPD. CNTs/LSCF composite coatings of high structural homogeneity were obtained by EPD from suspensions containing a 1:10 CNTs/LSCF ratio (in weight) and pH 4.8. The voltage used was 25 V and deposition time was 4 min. The challenges encountered to fabricate these composite layers by EPD were tackled investigating the different conditions of suspension preparation and stabilization coupled with CNTs funtionalization. It was found that the distribution of CNTs in the deposited LSCF matrix was homogeneous and the fabrication of a highly porous LSCF films by heat treatment of the deposits in air at 800°C was demonstrated for the first time in this study. The high porosity of the LSCF cathode would allow improving the electrochemical performance of the IT-SOFC cathodes; potencially enhancing the kinetic of the oxygen reduction reaction.

References

1. E. V. Tsipis and V. V. Kharton, "Electrode Materials and Reaction Mechanisms in Solid Oxide Fuel Cells: A Brief Review," *J. Solid State Electrochem.*, 12 1039–1060 (2008).
2. T. Yamaguchi, S. Shimizu, T. Suzuki, Y. Fujishiro, and M. Awano, "Fabrication and Characterization of High Performance Cathode Supported Small-Scale SOFC for Intermediate Temperature Operation," *Electrochem. Commun.*, 10 1381–1383 (2008).
3. M. Prestat, A. Infortuna, S. Korrodi, S. Rey-Mermet, P. Muralt, and L. Gauckler, "Oxygen Reduction at Thin Dense $La_{0.52}Sr_{0.48}Co_{0.18}Fe_{0.82}O_{3-\delta}$ Electrodes," *J. Electroceram.*, 18 111–120 (2007).
4. N. Grunbaum, L. Dessemond, J. Fouletier, F. Prado, and A. Caneiro, "Electrode Reaction of $Sr_{1x}La_xCo_{0.8}Fe_{0.2}O_{3\delta}$ with $x = 0.1$ and 0.6 on $Ce_{0.9}Gd_{0.1}O_{1.95}$ at $600 \leq T \leq 800$°C," *Solid State Ionics*, 177 907–913 (2006).
5. H. Ullmann, N. Trofimenko, F. Tietz, D. Stöver, and A. Ahmad-Khanlou, "Correlation Between Thermal Expansion and Oxide Ion Transport in Mixed Conducting Perovskite-Type Oxides for SOFC Cathodes," *Solid State Ionics*, 138 79–90 (2000).
6. S. B. Adler, "Factors Governing Oxygen Reduction in Solid Oxide Fuel Cell Cathodes," *Chem. Rev.*, 104 4791–4843 (2004).
7. A. V. Vikar, J. Chen, C. W. Tanner, and J. W. Kim, "The Role of Electrode Microstructure on Activation and Concentration Polarizations in Solid Oxide Fuel Cells," *Solid State Ionics*, 131 189–198 (2000).
8. E. P. Murray, M. J. Sever, and S. A. Barnett, "Electrochemical Performance of (La,Sr)(Co,Fe)O_3–(Ce,Gd)O_3 Composite Cathodes," *Solid State Ionics*, 148 27–34 (2002).

9. W. Guo, J. Liu, C. Jin, H. Gao, and Y. Zhanga, "Electrochemical Evaluation of $La_{0.6}Sr_{0.4}Co_{0.8}Fe_{0.2}O_{3-1}$–$La_{0.9}Sr_{0.1}Ga_{0.8}Mg_{0.2}O_{3-1}$ Composite Cathodes for $La_{0.9}Sr_{0.1}Ga_{0.8}Mg_{0.2}O_{3-1}$ Electrolyte SOFCs," *J. Alloys Compd.*, 473 43–47 (2008).
10. F. Qiang, K-N. Sun, N. Zhang, X-D. Zhu, X-D. Le, and D-R. Zhou, "Characterization of Electrical Properties of GDC Doped A-Site Deficient LSCF Based Composite Cathode using Impedance Spectroscopy," *J. Power Sources*, 168 338–345 (2007).
11. S. H. Iijima, "Helical Microtubules of Graphitic Carbon," *Nature*, 354 56–58 (1991).
12. T. Guo, P. Nikolaev, A. Thess, D. T. Colbert, and R. E. Smalley, "Catalytic Growth of Single-Walled Nanotubes by Laser Vaporization," *Chem. Phys. Lett.*, 243 49–54 (1995).
13. A. R. Boccaccini and I. Zitomirsky, "Application of Electrophoretic and Electrolytic Deposition Techniques in Ceramics Processing," *Curr. Opin. Solid State Mater. Sci.*, 6 251–260 (2002).
14. D. Beckel, A. Dubach, A. N. Grundy, A. Infortuna, and L. J. Gauckler, "Solid-State Dewetting of $La_{0.6}Sr_{0.4}Co_{0.2}Fe_{0.8}O_{3\pm\delta}$ Thin Films During Annealing," *J. Eur. Ceram. Soc.*, 28 49–60 (2008).
15. J. Will, A. Mitterdorfer, C. Kleinlogel, D. Perednis, and L. J. Gauckler, "Fabrication of Thin Electrolytes for Second-Generation Solid Oxide Fuel Cells," *Solid State Ionics*, 131 79–96 (2000).
16. L. Baqué and A. Serquis, "Microstructural Characterization of $La_{0.4}Sr_{0.6}Co_{0.8}Fe_{0.2}O_{3-\delta}$ Films Deposited by Dip Coating," *Appl. Surf. Sci.*, 254 213–218 (2007).
17. L. Baqué, A. Serquis, N. Grunbaum, F. Prado, and A. Caneiro, "Preparation and Characterization of Solid Oxide Fuel Cells Cathode Films," *Mater. Res. Soc. Symp. Proc.*, 928 181–186 (2006).
18. P. Sarkar and P. S. Nicholson, "Electrophoretic Deposition (EPD): Mechanisms, Kinetics, and Application to Ceramic," *J. Am. Ceram. Soc.*, 79 1987–2002 (1996).
19. L. Besra and M. Liu, "A Review on Fundamentals and Applications of Electrophoretic Deposition (EPD)," *Prog. Mater. Sci.*, 52 1–61 (2007).
20. H. Negishi, *et al.*, "Preparation of Thin and Dense Lanthanum Cobaltite Coating on Porous Tubular Alumina Supports by Electrophoretic Deposition," *J. Ceram. Soc. Jpn.*, 114 [1] 36–41 (2006).
21. I. Zhitomirsky and A. Petric, "Electrophoretic Deposition of Ceramic Materials for Fuel Cell Applications," *J. Eur. Ceram. Soc.*, 20 2055–2061 (2000).
22. A. R. Boccaccini, O. Van der Biest, and R. Clasen, eds. Electrophoretic Deposition: Fundamental and Applications II," *Key Eng. Mater.*, 314 1–267 (2006).
23. A. R. Boccaccini, J. Cho, J. A. Roether, B. J. C. Thomas, E. J. Minay, and M. S. P. Shaffer, "Electrophoretic Deposition of Carbon Nanotubes: Review," *Carbon*, 44 3149–3160 (2006).
24. C. S. Du, D. Heldbrant, and N. Pan, "Preparation and Preliminary Property Study of Carbon Nanotubes Films by Electrophoretic Deposition," *Mater. Lett.*, 57 [2] 434–438 (2002).
25. F. Chicatún, *et al.*, "Carbon Nanotube Deposits and CNT/SiO_2 Composite Coatings by Electrophoretic Deposition," *Adv. in Appl. Ceram.*, 106 [4] 186–195 (2007).
26. I. Singh, C. Kaya, M. S. P. Shaffer, B. C. Thomas, and A. R. Boccaccini, "Bioactive Ceramic Coatings Containing Carbon Nanotubos on Metallic Substrates by Electrophoretic Deposition," *J. Mater. Sci.*, 41 8144–8151 (2006).
27. S. V. Mahajan, S. A. Hasan, J. Cho, M. S. P. Shaffer, A. R. Boccaccini, and J. H. Dickerson, "Carbon Nanotube–Nanocrystal Heterostructures Fabricated by Electrophoretic Deposition," *Nanotechnology*, 19 195301 (2008).
28. M. J. Santillán, A. Caneiro, N. Quaranta, and A. R. Boccaccini, "Electrophoretic Deposition of $La_{0.6}Sr_{0.4}Co_{0.8}Fe_{0.2}O_{3-\delta}$ Cathodes on $Ce_{0.9}Gd_{0.1}O_{1.95}$ Substrates for Intermediate Temperature Solid Oxide Fuel Cell (IT-SOFC)," *J. Eur. Ceram. Soc.*, 29 1125–1132 (2008).
29. P. Lenormand, S. Castillo, J. R. Gonzalez, C. Robert, and F. Ansart, "Lanthanum Ferromanganites Thin Films by Sol–Gel Process. Influence of the Organic/Inorganic R Ratio on the Microstructural Properties," *Solid State Sci.*, 7 159–163 (2005).
30. M. L. Fontaine, *et al.*, "Synthesis of $La_2NiO_{4+\delta}$ Oxides by Sol–Gel Process: Structural and Microstructural Evolution from Amorphous to Nanocrystallized Powders," *Mater. Res. Bull.*, 41 1747–1753 (2006).
31. M. S. Shaffer, X. Fan, and A. H. Windle, "Dispersion and Packing of Carbon Nanotubes," *Carbon*, 36 [11] 1603–1612 (1998).
32. H. Kruidhof, H. J. M. Bouwmeester, R. H. E. Van Doorn, and A. Burggraf, "Influence of Order-Dissorder Transitions on Oxygen Permeability Through Selected Nonstoichiometric Perovskite-Type Oxides," *Solid State Ionics*, 63–65 816–822 (1993).
33. H. Dai, "Carbon Nanotubes: Opportunities and Challenges," *Surface Science*, 500 218–241 (2002).
34. B. J. C. Thomas, A. R. Boccaccini, and M. S. P. Shaffer, "Multi-Walled Carbon Nanotube Coatings Using Electrophoretic Deposition (EPD)," *J. Am. Ceram. Soc.*, 88 [4] 980–982 (2005).
35. H. Zhao, H. Song, Z. Li, G. Yuan, and Y. Jin, "Electrophoretic Deposition and Field Emission Properties of Patterned Carbon Nanotubes," *Appl. Surf. Sci.*, 251 242–244 (2005).
36. T. Ishihara, K. Shimose, T. Kudo, H. Nishiguchi, T. Akbay, and Y. Takita, "Preparation of Yttria-Stabilized Zirconia Thin Films on Strontium-Doped $LaMnO_3$ Cathode Substrates Via Electrophoretic Deposition for Solid Oxide Fuel Cells," *J. Am. Ceram. Soc.*, 83 1921–1927 (2000).
37. F. Chen and M. Liu, "Preparation of Yttria-Stabilized Zirconia (YSZ) Films on $La_{0.85}Sr_{0.15}MnO_3$ (LSM) and LSM–YSZ Substrates using an Electrophoretic Deposition (EPD) Process," *J. Eur. Ceram. Soc.*, 21 127–134 (2001).
38. M. J. Santillán, F. Membrives, N. Quaranta, and A. R. Boccaccini, "Characterization of TiO_2 Nanoparticle Suspensions for Electrophoretic Deposition," *J. Nanopart. Res.*, 10 787–793 (2008).
39. A. R. Boccaccini, P. Karapappas, J. M. Marijuan, and C. Kaya, "TiO_2 Coating on Silicon Carbide and Carbon Fibre Substrates by Electrophoretic Deposition," *J. Mater. Sci.*, 39 851–859 (2004).
40. S. T. Aruna and K. S. Rajam, "A Study on the Electrophoretic Deposition of 8YSZ Coating Using Mixture of Acetone and Ethanol Solvents," *Mater. Chem. & Phys.*, 111 131–136 (2008).
41. K. Esumi, M. Ishigami, A. Nakajima, K. Sawada, and H. Honda, "Chemical Treatment of Carbon Nanotubos: Review," *Carbon*, 34 [2] 279–281 (1996).
42. A. R. Boccaccini, P. A. Trusty, D. M. R. Taplin, and C. B. Ponton, "Colloidal Processing of a Mullite Matrix Material Suitable for Infiltrating Woven Fibre Preforms Using Electrophoretic Deposition," *J. Eur. Ceram. Soc.*, 16 1319–1327 (1996).
43. R. Castro, P. Marcos, E. Sakamoto, and D. Gouvea, "Surface Reactivity and Electrophoretic Deposition of ZrO_2–MgO Mechanical Mixture," *J. Mater. Sci.*, 42 6946–6954 (2007).
44. L. K. Koopal, *A Review of Coagulation and Flocculation: Theory and Applications*, vol. 47, eds., B. Dobias and M. Dekker, New York, 1993.
45. T. Ishihara, K. Sato, and Y. Takita, "Electrophoretic Deposition of Y_2O_3-Stabilized ZrO_2 Electrolyte Films in Solid Oxide Fuel Cells," *J. Am. Ceram. Soc.*, 79 913–919 (1996).
46. I. Corni, M. P. Ryan, and A. R. Boccaccini, "Electrophoretic Deposition: From Traditional Ceramics to Nanotechnology," *J. Eur. Ceram. Soc.*, 28 1353–1367 (2008).
47. K. Sasaki, J.-P. Wurth, R. Gscewend, M. Gödickemeier, and L. J. Gauckler, "Microstructure-Property Relations of Solid Oxide Fuel Cell Cathodes and Current Collectors," *J. Electrochem. Soc.*, 143 [2] 530–543 (1996).
48. H. S. Song, W. H. Kim, S. H. Hyun, J. Moon, J. Kim, and H-W. Lee, "Effect of Starting Particulate Materials on Microstructure and Cathodic Performance of Nanoporous LSM-YSZ Composite Cathodes," *J. Power Sources*, 167 258–264 (2007).